PCCP

PAPER

View Article Online
View Journal | View Issue

Cite this: *Phys. Chem. Chem. Phys.*, 2018, **20**, 6591

Gas-phase kinetics modifies the CCN activity of a biogenic SOA†

A. E. Vizenor [ab] and A. A. Asa-Awuku *[abc]

Received 4th January 2018,
Accepted 29th January 2018

DOI: 10.1039/c8cp00075a

rsc.li/pccp

Our current knowledge of cloud condensation nuclei (CCN) activity and the hygroscopicity of secondary organic aerosol (SOA) depends on the particle size and composition, explicitly, the thermodynamic properties of the aerosol solute and subsequent interactions with water. Here, we examine the CCN activation of 3 SOA systems (2 biogenic single precursor and 1 mixed precursor SOA system) in relation to gas-phase decay. Specifically, the relationship between time, gas-phase precursor decay and CCN activity of 100 nm SOA is studied. The studied SOA systems exhibit a time-dependent growth of CCN activity at an instrument supersaturation of ~0.2%. As such, we define a critical activation time, t_{50}, above which a 100 nm SOA particle will activate. The critical activation time for isoprene, longifolene and a mixture of the two precursor SOA is 2.01 hours, 2.53 hours and 3.17 hours, respectively. The activation times are then predicted with gas-phase kinetic data inferred from measurements of precursor decay. The gas-phase prediction of t_{50} agrees well with CCN measured t_{50} (within 0.05 hours of the actual critical times) and suggests that the gas-to-particle phase partitioning may be more significant for SOA CCN prediction than previously thought.

Introduction

The ability to become CCN and form a stable droplet depends on a particle's hygroscopicity and water activity. The term hygroscopicity characterizes the aerosol solute bulk composition. Hygroscopicity can be and is often quantified by the single parameter, κappa (κ), measured at sub and supersaturated relative humidities.[1] Traditionally, κappa values are assumed to be constant for aerosols of singular chemical composition. For secondary organic aerosol (SOA), comprised of thousands of compounds, few of which have been speciated,[2] the average κappa has values near ~0.1 and can increase with ageing.[1,3–9]

In several published cases, the apparent hygroscopicity of SOA can be dynamic and transient, although deviations within ±0.05 of the reported kappa values can be considered within the uncertainty of analysis.[10–13] Tang *et al.*[10] found that kappa of the amine SOA varied with supersaturation, whereas Zhao *et al.*[12] demonstrated a changing kappa value with changing O : C ratios (biogenic *versus* anthropogenic SOA precursors). However, Hildebrandt-Ruiz *et al.*[13] found that O : C and kappa did not appear to show a relationship, although the possibility of gas-phase surfactants may explain this. Recent studies have shown a direct dependence between κappa and the changing composition of SOA.[6,11,12] For example, Zhao *et al.*[11] demonstrated a size dependence of κappa with ageing. The changes in hygroscopicity were strongly correlated with changes in particle oxidation attributed to oxidation primarily occurring in the gas phase and whose products were partitioned between the particle phase and gas phase through condensation and evaporation.[11]

Due to instrumentation limitations, κappa values are often reported in specific times of ageing experiments. Particle diameters can shift to larger sizes beyond the window of instrument supersaturation and the critical electrical mobility diameter.[4,9,11,14] For example, Asa-Awuku *et al.*[4] explored the CCN activity of the β-caryophyllene SOA and noted a shift in the activation diameter over the course of the experiment. The CCN/CN ratio for 100 nm particles at 0.61% supersaturation increased sigmoidally over time as well. Vizenor *et al.*[14] showed that κ-hygroscopicity values could only be obtained in the initial stages of SOA formation and ageing for the longifolene SOA. Furthermore, the evolution of the longifolene SOA likely occurred from gas-phase autooxidation and CCN activity changed with time.[14] In the studies above, hygroscopicity changes are generally associated with the particle phase of aerosols, rather than the properties of the gas-phase precursors. Thermodynamic droplet theory is modified using the solute properties

[a] *Department of Chemical and Environmental Engineering, Bourns College of Engineering, University of California, Riverside, CA 92521, USA. E-mail: asaawuku@umd.edu*
[b] *Bourns College of Engineering, Center for Environmental Research and Technology (CE-CERT), Riverside, CA 92507, USA*
[c] *A. James Clark School of Engineering, Department of Chemical and Biomolecular Engineering, University of Maryland, College Park, MD 20742, USA*

† Electronic supplementary information (ESI) available. See DOI: 10.1039/c8cp00075a

(*e.g.* molecular weight, density, molar volume, *etc.*) and as such the aerosol solute properties are often explored in conjunction with CCN measurements.

The recent results of Zhao *et al.*[11] and Vizenor *et al.*[14] are indicative of a stronger and more influential role of gas-phase chemistry in SOA CCN. Here, we explore the role of gas-phase chemistry and CCN with a systematic study that relates the chemistry of the decay of gas-phase biogenic SOA precursors to CCN activity. Specifically, we present multiple datasets for SOAs formed from isoprene, longifolene and an atmospherically representative mixture of a monoterpene/sesquiterpene precursor with a hydroxyl radical. Longifolene is a less studied compound yet its slow decay allows for discrete measurement. Longifolene is not reactive with ozone;[15] thus excess hydroxyl radical photooxidation is employed to ensure that all precursors react. Several SOA and CCN studies tend to focus on single precursor SOA yields and oxidation states; singular precursor studies are useful for developing reaction mechanisms and the identification of compounds. Yet the atmosphere is a complex system with a plethora of VOC precursors and oxidants present at once. Multiple precursor studies contribute an added level of complexity that are characteristic of real-world emissions and reactions. Interactions between gas-phase VOC precursors, oxidants, and their subsequent reaction products are not well understood and may alter the chemical and physical properties of the resulting SOA CCN. The following work investigates the evolution of the SOA properties from single and multiple precursors with an emphasis on gas-phase kinetics and CCN activity.

Methods and instrumentation

Experiments were conducted at the University of California, Riverside, College of Engineering, Center for Environmental Research and Technology (UCR/CE-CERT), atmospheric chamber facility. Dual 90 m^3 Teflon reactors are housed in an insulated enclosure.[16] Temperature was kept constant at room temperature (21 °C), and relative humidity was maintained below 0.1% relative humidity (RH, LI-COR LI-840A CO_2/H_2O analyzer). The enclosure is continuously flushed with purified air (Aadco 737 series air purification system; Cleves, Ohio), and 272 115 W Sylvania black lights were used to simulate irradiation and UV light in the chamber. 2 ppm of H_2O_2 was injected in each experiment and provided a source of OH radicals. VOCs were then injected with target concentrations of ~100 ppb for isoprene and ~7 ppb for longifolene, to simulate the much larger concentration ratios of isoprene to sesquiterpenes commonly found in the environment.[17–19] UV lights were turned on after all injections were stabilized. Photooxidation lasted up to 8 hours and both gas and particle-phase properties were measured.

Gas-phase VOC precursor decay was quantified with an Agilent Gas Chromatograph-Flame Ionization Detector (GC-FID). Both longifolene and isoprene were detected using a GC-FID. Gas-phase data were collected every ~25 minutes. The terpene retention times during gas chromatography are distinct. Thus, isoprene and longifolene are an optimal choice for an experimental study; the possibility of redundancy in VOC concentration measurements with GC-FID is eliminated in multiple precursor experiments. In multiple precursor studies, the precursor concentration is reported as the sum of the precursors and individually for each precursor component.

A home built scanning mobility particle sizer (SMPS) measured the particle number concentration (27–685 nm size distributions).[20] The aerosol mass concentration was calculated by multiplying the measured SOA density, ρ (Aerosol Particle Mass Analyzer, APM, Kanomax model 3600) and the SMPS particle volume. Yield was then calculated with the one-product model,[21] defined as the ratio of particle mass produced (from SMPS, and APM data) to the amount of reactive gas species (consumed precursor from GC-FID data). The aerosol elemental composition and the oxidation state were also measured using an Aerodyne High Resolution Time-of-Flight Aerosol Mass Spectrometer (HR-ToF-MS).[22–24] Improved-ambient corrections were applied for O : C and H : C calculations.[24]

CCN activity was measured using a Droplet Measurement Technologies (DMT) Continuous-Flow Streamwise Thermal Gradient CCN Counter (CCNC).[25–27] Aerosol was classified with a commercial SMPS (TSI, 3080) and operated in parallel to a condensation particle counter (CPC, TSI 3772 or 3776) and the CCNC. 100 nm mobility diameter particles were selected and the ratio of activated CCN to total particles (condensation nuclei, CN) was observed at ~0.2% supersaturation (SS). For constant and known solute composition, the CCN/CN ratio at given particle diameters and supersaturations will not change (*i.e.*, CCN/CN ratio of $(NH_4)_2SO_4$ at 100 nm and 0.2% SS = 1); the kappa value is also constant as the solute composition does not change. The reported SS for each experiment was derived from instrument calibration with $(NH_4)_2SO_4$. Each calibration determined critical diameters to infer actual instrument SS (Fig. S1, ESI†). Data were also charge corrected to account for doubly-charged particles. The ESI† shows the charge corrected data for the measured size distribution (100 nm particles are also indicated). It is noted that the charge corrected size distribution of particles becomes more CCN active during the ageing experiment.

Results and discussion

In all experiments, SOAs are substantially formed from subsequent CCN measurements. While sesquiterpenes are known to produce high yields of aerosols (>50%), isoprene generally does not produce yields greater than 8%.[14,28] Here, the average yield of longifolene and isoprene SOAs is 60% and 13%, respectively. Despite the low yield of the isoprene SOA and small precursor concentrations of the longifolene SOA, enough SOA is produced for physical and chemical particle measurements (*e.g.*, 19 μg m^{-3} and 50 μg m^{-3} for the isoprene SOA and longifolene SOA, respectively). The average SOA yield of the isoprene + longifolene precursor mixture is 25%. The SOA yield is consistent with previous sesquiterpene and isoprene SOA

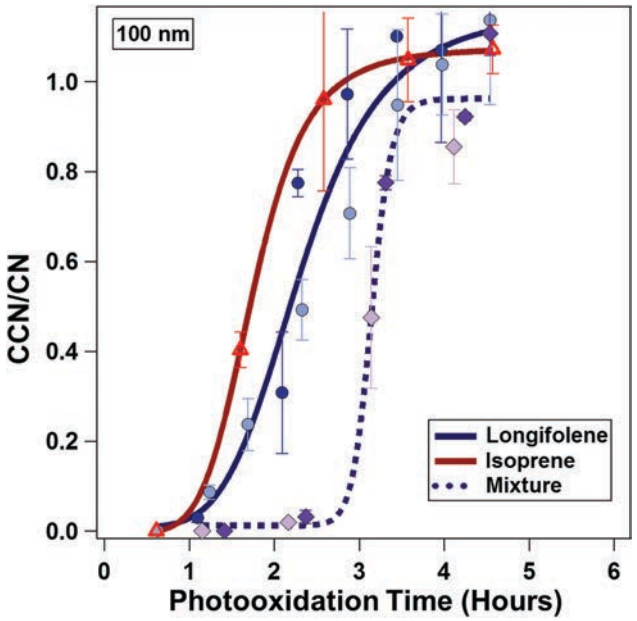

Fig. 1 CCN/CN activation ratio of 100 nm SOA Particles *versus* time. Multiple measurements of isoprene SOA (red triangles), longifolene SOA (blue circles) and isoprene + longifolene mixture SOA (purple diamonds) are shown. Lines are the average best fit sigmoid as presented in eqn (1).

formation yields.[9] Furthermore, both studies show that small amounts of sesquiterpenes in the presence of isoprene increase reactivity, leading to non-additive higher SOA yields.

SOA nucleation and formation begins 20 minutes after the initiation of photooxidation. At that time, 100 nm are present in sufficient concentrations (>50 #/cc). The average CCN/CN ratio of 100 nm particles of the longifolene SOA, isoprene SOA and isoprene + longifolene SOA is plotted in Fig. 1 at 0.24% SS. The CCN/CN ratio is plotted *versus* particle electrical mobility diameter or SS, and the point of inflection on the sigmoid is the critical dry diameter or critical supersaturation, above which particles will rapidly activate as CCN.[1,29] A similar sigmoid can be applied to plot CCN/CN *versus* time for a given particle diameter and SS as follows:

$$\frac{\mathrm{CCN}}{\mathrm{CN}} = S_{\min} + \frac{S_{\max} - S_{\min}}{1 + \left[\frac{t_{50\mathrm{ccn}}}{t}\right]^{r}} \quad (1)$$

where $S_{\min}$ is the minimum value of the bottom plateau's sigmoid, $S_{\max}$ is the maximum plateau value, $t_{50\mathrm{ccn}}$ is the critical time at which 50% of the particles activate as CCN, t is the time at which measurements are taken and r is the rate at which the sigmoid increases. Theoretically, $S_{\min}$ and $S_{\max}$ are equal to 0 and 1, respectively, as there are no CCN active particles at the beginning of the experiment (CCN/CN = 0). Later, if the particle is sufficiently hygroscopic, all of the particles activate as CCN. The most important sigmoidal variables for SOAs are $t_{50\mathrm{ccn}}$ and r, as these variables can be unique to specific SOA precursors. $t_{50\mathrm{ccn}}$ values of isoprene, longifolene and the SOA mixture are 1.95, 2.53 and 3.17 hours, respectively (Table 1). The critical times for activation appear to be distinct for the three separate systems.

Table 1 Time dependent CCN SOA properties of 100 nm particles

	k	Base	Max	Rate	$\left(\frac{kt}{C_A^{1-n}}\right)^{50}$	$t_{50,\mathrm{gas}}$ (h)	$t_{50,\mathrm{ccn}}$ (h)
Longifolene	0.87 h^{-1}	0.01	1.15	2.01	2.01	2.31	2.15
Isoprene	1.03 h^{-1}	0.00	1.07	1.80	1.80	1.74	1.75
Mixture	0.22 $ppm^{(0.25)}$ h^{-1}	0.01	0.96	18.5	1.60	3.00	3.15

Furthermore, the critical time for 100 nm particles to form CCN active materials in the multiple-precursor SOA system is longer than that of the single-precursor SOA. r, the rate at which the sigmoid increases is similar for individual precursors (~2) but significantly larger for the SOA mixture. The SOA from the precursor mixture rapidly becomes active after $t_{50\mathrm{ccn}}$.

Changes in the particle CCN activity are likely due to chemical changes (either in the bulk or the surface) of the aerosol. Again, the effects of doubly charged particles have been accounted for (Fig. S1, ESI†). Yet the additional physical and chemical aerosol data available for this study provide little information about the rapid change in CCN activity after $t_{50\mathrm{CCN}}$. For example, the density of the SOAs from isoprene, longifolene and the terpene mixture SOA remains constant (1.3 ± 0.1) during experiments. The bulk O:C and H:C ratios from AMS data provide some insights into the changing chemical properties of 100 nm particles but do not exhibit rapid changes (Fig. 2). In Fig. 2, longifolene has lower O:C and H:C (~0.24 and 1.6, respectively) and isoprene has higher values (0.7 and 1.95). The oxidation state of the mixture does discernibly change with time (Fig. 2). At the start of isoprene + longifolene SOA formation, the mixture appears higher on the Van Krevelen plot, similar to the isoprene SOA oxidation state. However, as the reaction progresses, the O:C and H:C ratios decrease by ~0.2, and appear more like a longifolene SOA. The AMS data of the SOA mixture are consistent with yield calculations and suggest that small amounts of longifolene may contribute to the composition and functionality of the SOA as the reaction progresses. Yet, it is noted that

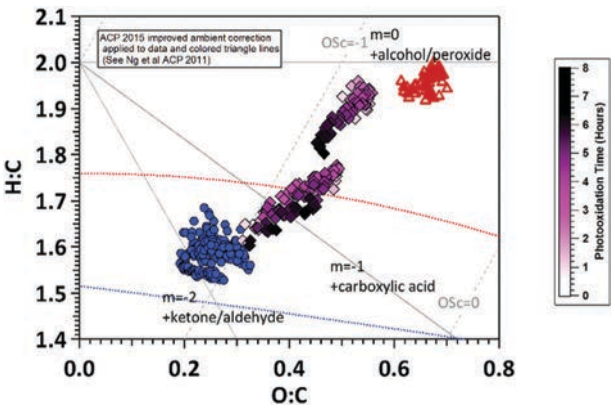

Fig. 2 Van Krevelen diagram of biogenic SOA systems. HR-AMS measurements of isoprene SOA (red triangles), longifolene SOA (blue circles) and isoprene + longifolene mixture SOA (diamonds) are shown. The transition of the isoprene + longifolene mixture SOA with time are shown for two distinct experiments. Isoprene, and longifolene SOA systems do not significantly change with time.

the HR-AMS aerosol chemical information presented is limited with regard to the CCN activation of 100 nm particles; it is not single-particle chemistry data and the AMS aerodynamic lens provides bulk chemistry information skewed for particles $> \sim 60$ nm in the electrical mobility diameter. Consistent with previous studies, O : C only provides an approximate guide to particle hygroscopicity.[30]

The gas-phase chemical decay however is consistent with the time scale of aerosol formation and ageing. In all experiments, more than 95% of the initial gas-phase precursor was consumed by the end of the experiment. The single-precursor decay of longifolene and isoprene was assumed to fit a simple first-order exponential decay.[31,32] The assumptions are validated by plotting the natural logarithm of the ratio of the precursor concentration divided by the initial precursor concentration as a function of photooxidation time and forcing the best fit through zero (Fig. 3(top), see the ESI† for the kinetic derivation). The slope of the linear fit corresponds to an observed reaction constant, k (Table 1). k values are not absolute and are specific to the conditions of the chamber system. Additionally, k values are not corrected for particle formation known to influence gas-phase reactions.[15,28,29] Longifolene (as expected) had a slower decay rate than that of isoprene. The measured data agree well with the first-order assumption (Fig. 3(top), $R^2 = 0.97$ and 0.98, isoprene and longifolene, respectively). This same experimental protocol and analysis was then applied to the more complex multiple precursor studies.

In multiple precursor experiments, the time for individual precursor decay was significantly longer (almost double) in the presence of excess H_2O_2 (2 ppm). The measured concentrations of isoprene and longifolene in the multiple precursor experiments did not exhibit first-order decay; the resulting fit of the first order model resulted in lower correlations for isoprene and longifolene ($R^2 = 0.59$ and $R^2 = 0.67$, respectively). This change in the observed pseudo-reaction order suggests a non-additive precursor behaviour and the possibility of gas-phase cross reactions between oxidation products. As such, a kinetic model assuming overall pseudo-nth order kinetics was applied to the multiple-component system and individual precursors in the mixed precursor experiment. These decays were also plotted using two first-order decay fits and the analysis is presented in the ESI.†

To estimate the order of the reaction for multiple precursors, nth order kinetic analysis was performed by plotting the ratio of gas-phase concentrations, $\frac{C^{1-n}}{C_0^{1-n}}$, *versus* photooxidation time (Fig. 3(bottom)). The value of the pseudo-order, n, was obtained from a best-fit linear regression (see the ESI† for derivation and additional details). The nth order kinetic analysis estimates that the observed overall order of the reaction for the isoprene + longifolene SOA is 0.75 (Fig. 3(bottom)) and is less than 1 and is consistent with a slower decay of precursors. A similar analysis is applied to the individual precursors and shows that the overall kinetics are non-elementary; longifolene decays with the 0.5 order and isoprene decays with the 0.75 order. Notably, the best fit of the overall reaction order is similar to that of isoprene, further suggesting that isoprene plays a significant

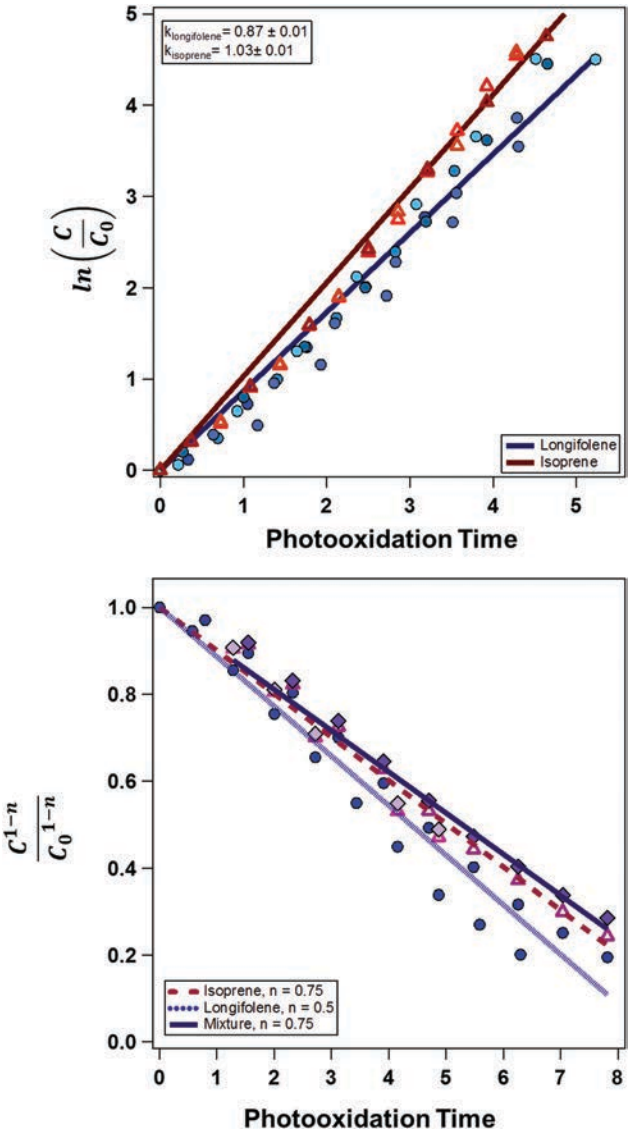

Fig. 3 Normalized gas-phase kinetic decay (top) single precursor decay of isoprene (red triangles) and longifolene SOA (blue circles) experiments. Assuming pseudo-first order kinetics, a best fit linear regression through the origin is applied to isoprene and longifolene (red, and blue lines, respectively) (bottom) overall precursor decay of isoprene + longifolene SOA mixtures (purple diamonds) and individual decay of isoprene (red triangles) and longifolene (blue circles) within the mixture. The total precursor concentration is the sum of isoprene and longifolene. The multiple-precursor system does not follow first order kinetics and is thus plotted assuming nth-order kinetics.

role, driving the overall reactivity of the system. The pseudo-nth order kinetics provides a more robust mathematical description of the gas-phase kinetics compared to the two-parameter fit first-order decay. The apparent reaction constant, k_{OH}, as estimated from the respective nth-order analysis is reported for single and multiple-precursor SOA systems (Table 1). For longifolene, the k_{OH} values were 0.87 h^{-1} and 0.0245 $ppm^{0.5}$ h^{-1} for single and multiple precursor reactions, respectively. Isoprene k_{OH} values were 1.03 h^{-1} and 0.2331 $ppm^{0.25}$ h^{-1}. The overall k_{OH} for the multiple precursor reactions was 0.220 $ppm^{0.25}$ h^{-1} and is similar

to that of isoprene in the system. Again, the similarity in the apparent reaction constant of the complex precursor mixture with k_{OH} of isoprene in the mixture strongly indicates that isoprene plays a significant role in the gas-phase chemistry and subsequent aerosol formation in the mixed isoprene + longifolene oxidation experiment.

The gas-phase decay as described above can be related to changes in the CCN activity of 100 nm particles. In pseudo first-order systems (*i.e.*, isoprene and longifolene SOA), the reactant concentration during decay can be normalized as follows:

$$-\left(\ln\frac{C}{C_0}\right) = kt \qquad (2)$$

where C is the precursor concentration at time, t, and C_0 is the initial concentration. It should be noted that the first-order normalized decay is non-dimensional and equivalent to kt (the reaction rate constant multiplied by time). The CCN/CN ratio for 100 nm particles at 0.24% SS was then plotted *versus* the normalized gas-phase decay (Fig. 4) estimated from kinetic parameters (Fig. 3). In Fig. 1 the CCN activity of the isoprene SOA and the longifolene SOA is distinct. When normalized for gas-phase kinetics, the sigmoidal fits of the isoprene SOA and longifolene SOA are almost identical (Fig. 4); strongly indicating that the gas-phase kinetics drives the apparent change in hygroscopicity of the 100nm particle.

For an nth order system, kt is calculated as follows:

$$kt = \frac{\left(\frac{C_A}{C_{A0}}\right)^{n-1} - 1}{n-1} \qquad (3)$$

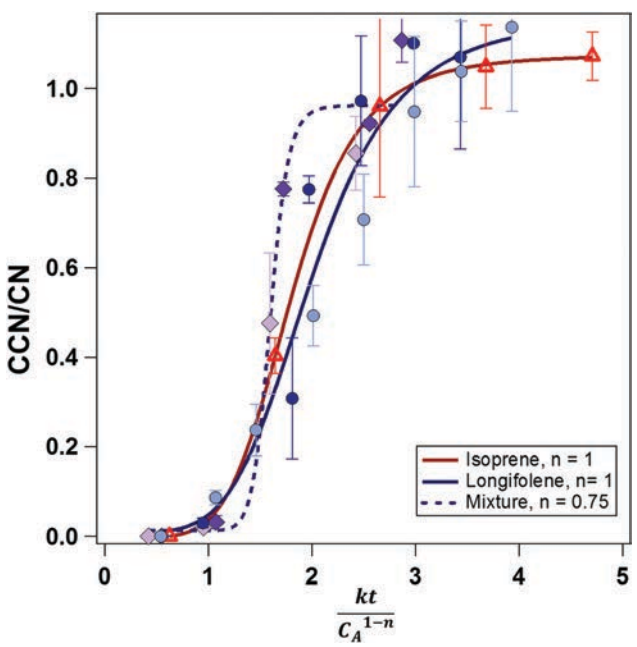

Fig. 4 CCN/CN activation ratio of 100 nm SOA particles *versus* dimensionless decay. Isoprene SOA (red triangles), longifolene SOA (blue circles) and isoprene + longifolene mixture SOA (purple diamonds) are shown. For first order systems, the apparent change in the CCN activity with normalized gas-phase decay is similar.

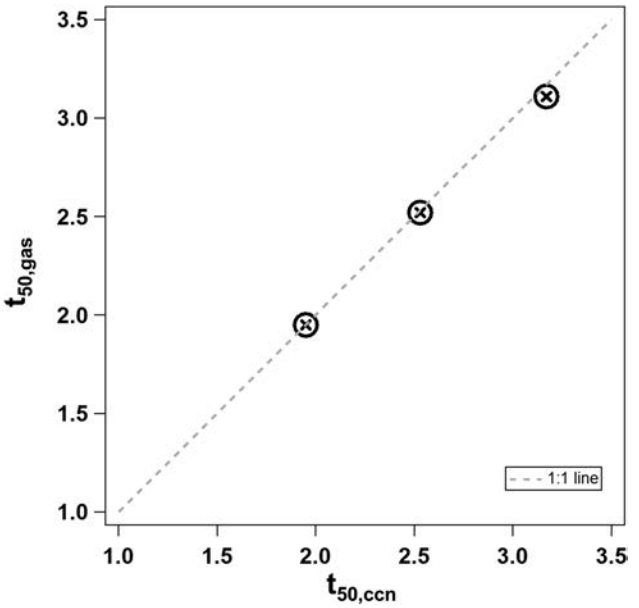

Fig. 5 Comparison of the gas-phase predicted critical time, $t_{50,gas}$ and CCN critical time, $t_{50,ccn}$.

In this case (for $n \neq 1$), kt is not dimensionless and has dimensions of $[ppm]^{0.25}$. To directly compare the gas-phase CCN analysis, all the data sets were plotted on a dimensionless x-axis, $\frac{kt}{C_A^{1-n}}$ (Fig. 4). The normalized CCN activity of a multiple-precursor SOA system (which activated at longer times in Fig. 1) is now similar to the single precursor sigmoids presented in Fig. 4.

One important observation from gas-phase normalized CCN analysis is the rate at which the 100 nm particles become fully CCN active. The sigmoids have more similar rates (5.29 ± 1.47 for isoprene, 6.245 ± 3.49 for longifolene and 7.31 ± 3.45 for the mixture), indicating a similarity in how quickly the particles activate once normalized by a dimensionless gas-phase kinetic time. These slopes are relatively small; the activation process is gradual upon reaching the critical time point.

An estimated t_{50} is inferred; that is, sigmoidal fits (eqn (1)) were applied to Fig. 4. The critical time (now inferred from gas-phase parameters), defined as t_{50gas}, was calculated and compared to t_{50ccn} (Fig. 5 and Table 1). The calculated t_{50gas} values for isoprene, longifolene and the mixture were 1.95, 2.52 and 3.11 hours, respectively. The t_{50gas} values agree well with t_{50ccn} (Fig. 5, within 0.05 hours), showing that temporal changes in the CCN activity are reproduced using gas-phase decay information.

Conclusions

The data presented here confirm the significance of gas-to-aerosol phase partitioning for CCN and reiterates the need to account for gas-phase chemistry in addition to particle phase chemistry for secondary aerosol systems. It is commonly assumed that the particle-phase is the main (sometimes sole) driver in the SOA CCN activity. CCN theory depends on the solute properties

however the complete solute composition of the SOA is unknown, difficult to speciate and thus the required thermodynamic properties for prediction are incomplete.

Additionally, changes in the observed aerosol composition and oxidation state (*e.g.* but not limited to aerosol density, O : C and H : C) are observed to correlate with changes in the CCN activity but the magnitude of changes is often small and does not capture the non-linear CCN behaviour of particles of a given size. Yet by using the gas-phase decay of the SOA precursors (whose initial emissions can be estimated and measured), we were able to normalize the effects of oxidation and recreate the critical CCN times found with photooxidation time. The observed relationship indicates that gas-phase vapors play an important role in the CCN activity. Acquiring information about the known gas-phase precursor source and subsequent decay can be used for the prediction of timescales of the CCN activity.

The uniqueness of these findings should be applied with caution as the results and analysis are most sensitive to the particle size selected. That is, for much smaller or larger particles at different SS, a sigmoidal response may not be observed with ageing. Nonetheless, 100 nm particles are of critical atmospheric size and relevance; often represented in new particle formation modeling efforts and considered a minimum hygroscopicity particle size for cloud microphysical models.[33–35] Indeed, if a critical time is required for activation, 100 nm SOA particles may not be assumed as instantaneous CCN.

Moreover, this work shows that multiple precursors influence the gas-phase kinetics for SOA formation. The change in gas-phase chemistry and kinetics subsequently modifies CCN activity. The pseudo-reaction order of the isoprene + longifolene SOA experiments is a non-integer value in the presence of excess OH. This suggests that with multiple precursors, cross-linking reactions in the gas-phase could occur thus altering the overall perceived order of reaction. This change in kinetics affects the properties of SOA relating to hygroscopicity and the added complexity of reactions in the gas-phase can delay the formation of hygroscopic compounds in the aerosol phase. Isoprene appears to drive the gas-phase reactivity in the presence of small amounts of sesquiterpene, as the overall order of the reaction and the reaction rate constant, k, are similar to that of singular isoprene decay in the mixed system. This is also evidenced by the H : C and O : C ratios from the HR-ToF-AMS data, in which the multiple precursor SOA is initially similar to isoprene, and decreases in the value over time, behaving more like longifolene. It is likely that with isoprene dominating in the gas-phase reactivity of the system, longifolene simply enhances the reactivity further by increasing the SOA yield. The results thus imply that isoprene may significantly contribute to SOA and CCN budgets more than originally assumed. Furthermore, the ability of 100 nm SOA to be CCN active will not solely depend on the size and will be photooxidation time and gas-phase reaction dependent.

Conflicts of interest

There are no conflicts to declare.

Acknowledgements

Funding for this project was supported by the National Science Foundation Award (1151893). This work is the sole responsibility of the grantee and does not represent the official views of any funding agencies.

Notes and references

1 M. D. Petters and S. M. Kreidenweis, A single parameter representation of hygroscopic growth and cloud condensation nucleus activity, *Atmos. Chem. Phys.*, 2007, **7**, 1961–1971.
2 M. Kanakidou, *et al.*, Organic aerosol and global climate modelling: a review, *Atmos. Chem. Phys.*, 2005, **5**, 1053–1123.
3 G. J. Engelhart, A. Asa-Awuku, A. Nenes and S. N. Pandis, CCN activity and droplet growth kinetics of fresh and aged monoterpene secondary organic aerosol, *Atmos. Chem. Phys.*, 2008, **8**, 3937–3949.
4 A. Asa-Awuku, G. J. Engelhart, B. H. Lee, S. N. Pandis and A. Nenes, Relating CCN activity, volatility, and droplet growth kinetics of β-caryophyllene secondary organic aerosol, *Atmos. Chem. Phys.*, 2009, **9**, 795–812.
5 J. L. Jimenez, *et al.*, Evolution of organic aerosols in the atmosphere, *Science*, 2009, **326**, 1525–1529.
6 A. T. Lambe, *et al.*, Laboratory studies of the chemical composition and cloud condensation nuclei (CCN) activity of secondary organic aerosol (SOA) and oxidized primary organic aerosol (OPOA), *Atmos. Chem. Phys.*, 2011, **11**, 8913–8928.
7 T. Tritscher, *et al.*, Volatility and hygroscopicity of aging secondary organic aerosol in a smog chamber, *Atmos. Chem. Phys.*, 2011, **11**, 11477–11496.
8 J. P. S. Wong, *et al.*, Oxidation of ambient biogenic secondary organic aerosol by hydroxyl radicals: Effects on cloud condensation nuclei activity, *Geophys. Res. Lett.*, 2011, **38**, L22805.
9 X. Tang, D. R. Cocker, III and A. Asa-Awuku, Are sesquiterpenes a good source of secondary organic cloud condensation nuclei (CCN)? Revisiting β-caryophyllene CCN, *Atmos. Chem. Phys.*, 2012, **12**, 8377–8388.
10 X. Tang, *et al.*, Cloud condensation nuclei (CCN) activity of aliphatic amine secondary aerosol, *Atmos. Chem. Phys.*, 2014, **14**, 5959–5967.
11 D. F. Zhao, *et al.*, Size-dependent hygroscopicity parameter (κ) and chemical composition of secondary organic cloud condensation nuclei, *Geophys. Res. Lett.*, 2015, **42**, 10920–10928.
12 D. F. Zhao, *et al.*, Cloud condensation nuclei activity, droplet growth kinetics, and hygroscopicity of biogenic and anthropogenic secondary organic aerosol (SOA), *Atmos. Chem. Phys.*, 2016, **16**, 1105–1121.
13 L. Hildebrandt Ruiz, *et al.*, Formation and aging of secondary organic aerosol from toluene: changes in chemical composition, volatility, and hygroscopicity, *Atmos. Chem. Phys.*, 2015, **15**, 8301–8313.
14 A. Vizenor, S. A. K. Häme, I. Riipinen and A. Asa-Awuku, Volatility and hygroscopicity of longifolene SOA from hydroxyl radical chemical pathways, under review.

15 Y. Shu and R. Atkinson, Atmospheric lifetimes and fates of a series of sesquiterpenes, *J. Geophys. Res.*, 1995, **100**, 7275–7281.
16 W. P. L. Carter, in *Environmental Simulation Chambers: Application to Atmospheric Chemical Processes*, ed. I. Barnes and K. J. Rudzinski, Springer Netherlands, 2006, pp. 27–41.
17 J. Bai, *et al.*, Seasonal variations in whole-ecosystem BVOC emissions from a subtropical bamboo plantation in China, *Atmos. Environ.*, 2016, **124**(part A), 12–21.
18 A. B. Guenther, *et al.*, The Model of Emissions of Gases and Aerosols from Nature version 2.1 (MEGAN2.1): an extended and updated framework for modeling biogenic emissions, *Geosci. Model Dev.*, 2012, **5**, 1471–1492.
19 A. Guenther, *et al.*, A global model of natural volatile organic compound emissions, *J. Geophys. Res.*, 1995, **100**, 8873–8892.
20 D. R. Cocker, 3rd, R. C. Flagan and J. H. Seinfeld, State-of-the-art chamber facility for studying atmospheric aerosol chemistry, *Environ. Sci. Technol.*, 2001, **35**, 2594–2601.
21 Jay R. Odum, *et al.*, Gas/Particle Partitioning and Secondary Organic Aerosol Yields, *Environ. Sci. Technol.*, 1996, **30**, 2580–2585.
22 Peter F. DeCarlo, *et al.*, Field-Deployable, High-Resolution, Time-of-Flight Aerosol Mass Spectrometer, *Anal. Chem.*, 2006, **78**, 8281–8289.
23 J. L. Jimenez, *et al.*, Ambient aerosol sampling using the Aerodyne Aerosol Mass Spectrometer, *J. Geophys. Res.*, 2003, **108**, 8425.
24 M. R. Canagaratna, *et al.*, Elemental ratio measurements of organic compounds using aerosol mass spectrometry: characterization, improved calibration, and implications, *Atmos. Chem. Phys.*, 2015, **15**, 253–272.
25 S. Lance, A. Nenes, J. Medina and J. N. Smith, Mapping the Operation of the DMT Continuous Flow CCN Counter, *Aerosol Sci. Technol.*, 2006, **40**, 242–254.
26 G. C. Roberts and A. Nenes, A Continuous-Flow Streamwise Thermal-Gradient CCN Chamber for Atmospheric Measurements, *Aerosol Sci. Technol.*, 2005, **39**, 206–221.
27 D. Rose, *et al.*, Calibration and measurement uncertainties of a continuous-flow cloud condensation nuclei counter (DMT-CCNC): CCN activation of ammonium sulfate and sodium chloride aerosol particles in theory and experiment, *Atmos. Chem. Phys.*, 2008, **8**, 1153–1179.
28 J. H. Kroll, N. L. Ng, S. M. Murphy, R. C. Flagan and J. H. Seinfeld, Secondary organic aerosol formation from isoprene photooxidation, *Environ. Sci. Technol.*, 2006, **40**, 1869–1877.
29 R. H. Moore, A. Nenes and J. Medina, Scanning Mobility CCN Analysis – A Method for Fast Measurements of Size-Resolved CCN Distributions and Activation Kinetics, *Aerosol Sci. Technol.*, 2010, **44**, 861–871.
30 A. M. J. Rickards, R. E. H. Miles, J. F. Davies, F. H. Marshall and J. P. Reid, Measurements of the sensitivity of aerosol hygroscopicity and the κ parameter to the O/C ratio, *J. Phys. Chem. A*, 2013, **117**, 14120–14131.
31 M. Ghalaieny, *et al.*, Determination of gas-phase ozonolysis rate coefficients of a number of sesquiterpenes at elevated temperatures using the relative rate method, *Phys. Chem. Chem. Phys.*, 2012, **14**, 6596–6602.
32 S. Richters, H. Herrmann and T. Berndt, Highly Oxidized RO2 Radicals and Consecutive Products from the Ozonolysis of Three Sesquiterpenes, *Environ. Sci. Technol.*, 2016, **50**, 2354–2362.
33 U. Dusek, *et al.*, Enhanced organic mass fraction and decreased hygroscopicity of cloud condensation nuclei (CCN) during new particle formation events, *Geophys. Res. Lett.*, 2010, **37**, L03804.
34 C. E. Scott, *et al.*, Impact of gas-to-particle partitioning approaches on the simulated radiative effects of biogenic secondary organic aerosol, *Atmos. Chem. Phys.*, 2015, **15**, 12989–13001.
35 D. M. Westervelt, L. W. Horowitz, V. Naik, J.-C. Golaz and D. L. Mauzerall, Radiative forcing and climate response to projected 21st century aerosol decreases, *Atmos. Chem. Phys.*, 2015, **15**, 12681–12703.